

Three-dimensional viscoelastic finite element model for postseismic deformation of the great 1960 Chile earthquake

Y. Hu,¹ K. Wang,^{2,3} J. He,² J. Klotz,⁴ and G. Khazaradze⁵

Received 4 May 2004; revised 14 September 2004; accepted 1 October 2004; published 7 December 2004.

[1] We develop a three-dimensional viscoelastic finite element model to study postseismic deformation associated with the 1960 great Chile earthquake. GPS observations 35 years after the earthquake show that, while all coastal sites are moving landward, a group of inland sites 200–400 km from the trench are moving seaward and that coastal velocities in the 1960 rupture area are distinctly smaller than those to the north. We explain these observations in terms of mantle stress relaxation. The earthquake stretches the upper plate to move seaward, but elastic stresses coseismically induced in the upper mantle resist this motion. Stress relaxation allows seaward motion to take place in the inland area for several decades following the earthquake. With a viscosity of 2.5×10^{19} Pa s for the continental upper mantle, the model well explains the GPS observations. Numerical tests suggest that the continental mantle viscosity value is reasonably well constrained. The model shows the prolonged postseismic seaward motion of the inland area to be a unique feature of earthquakes with very long rupture along strike and large coseismic fault slip. For short rupture and small coseismic slip, the motion will stop very quickly after the earthquake, explaining why this phenomenon is not more commonly observed. With an oceanic mantle viscosity of 10^{20} Pa s, the model also provides an explanation for tide-gauge constrained postseismic uplift 200 km from the trench that had previously been explained using a model of prolonged afterslip of a deep segment of the Chile subduction fault. **INDEX TERMS:** 1236 Geodesy and Gravity: Rheology of the lithosphere and mantle (8160); 1242 Geodesy and Gravity: Seismic deformations (7205); 3230 Mathematical Geophysics: Numerical solutions; 7209 Seismology: Earthquake dynamics and mechanics; 7260 Seismology: Theory and modeling; **KEYWORDS:** postseismic deformation, viscoelastic stress relaxation, GPS, finite element modeling, Chile subduction zone, upper mantle viscosity

Citation: Hu, Y., K. Wang, J. He, J. Klotz, and G. Khazaradze (2004), Three-dimensional viscoelastic finite element model for postseismic deformation of the great 1960 Chile earthquake, *J. Geophys. Res.*, 109, B12403, doi:10.1029/2004JB003163.

1. Introduction

[2] To use geodetic data to investigate subduction dynamics and earthquake hazard, it is important to understand how the Earth's rheology controls the deformation process in subduction earthquake cycles. Deformation models applied to explain geodetic observations often assume that the subduction system is purely elastic, and therefore the deformation of the crust instantaneously responds to the motion of the fault, and any time dependence of the deformation is attributed to time-dependent fault slip.

However, in the real Earth, the mantle and possibly the lower crust as well approximate a Maxwell viscoelastic behavior; that is, any imposed stress will relax with time. In response to a subduction earthquake, the crust will first deform as an elastic body, but the deformation will continue because of stress relaxation [Thatcher and Rundle, 1984; Cohen, 1994; Wang, 2004]. For this reason, the strain accumulation and release process throughout subduction earthquake cycles has a complex time-dependent behavior. In this work, we employ viscoelastic finite element modeling to study postseismic crustal deformation associated with the 1960 Chile earthquake of M_w (moment magnitude) 9.5. Following Savage [1983] and many other workers, we only model the perturbation field associated with the earthquake process, and steady subduction and other long-term geological processes are assumed not to result in significant deformation at a decadal timescale.

[3] "Relaxation" means that stress decreases with time subject to an externally imposed and fixed displacement field. A schematic model in Figure 1a is used to illustrate the effect of stress relaxation. Trench-normal displacements along surface line AB in response to an instantaneous (coseismic) fault slip are schematically shown in

¹School of Earth and Ocean Sciences, University of Victoria, Victoria, British Columbia, Canada.

²Pacific Geoscience Centre, Geological Survey of Canada, Sidney, British Columbia, Canada.

³Also at School of Earth and Ocean Sciences, University of Victoria, Victoria, British Columbia, Canada.

⁴GeoForschungsZentrum Potsdam, Kinematics/Neotectonics, Telegrafenberg, Potsdam, Germany.

⁵Department of Geodynamics and Geophysics, University of Barcelona, Barcelona, Spain.

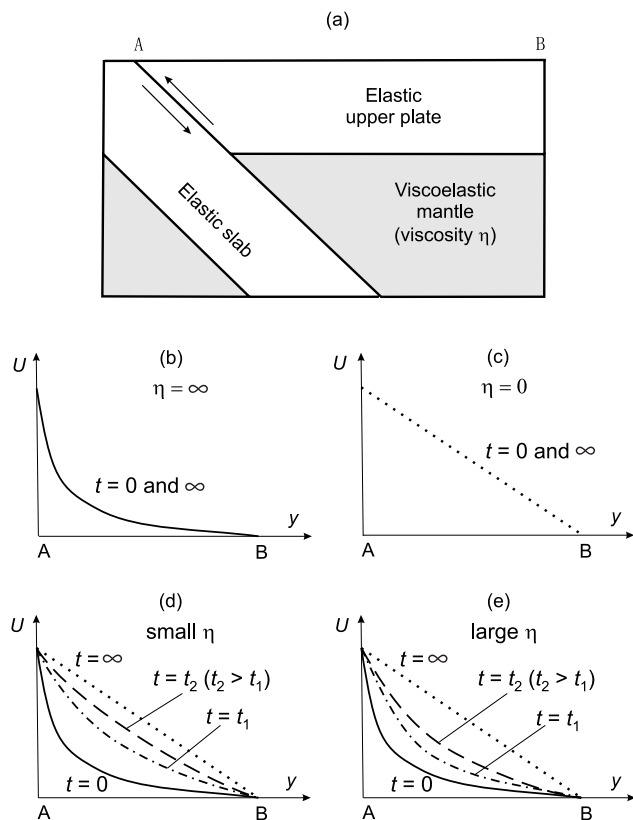


Figure 1. Crustal deformation in response to a single subduction earthquake. The effect of plate convergence is ignored in this schematic illustration. (b–e) Deformation with different upper mantle viscosities η . (a) U is trench-normal seaward displacement along line AB. Here t denotes time, and t_1 and t_2 represent two different time points.

Figures 1b, 1c, 1d, and 1e ($t = 0$). Stress in a deformed purely elastic Earth (i.e., mantle viscosity $\eta = \infty$) never relaxes (Figure 1b). An inviscid mantle ($\eta = 0$) relaxes instantly (Figure 1c). With a finite η (Figures 1d and 1e), the coseismic deformation ($t = 0$) is the same as that of a purely elastic system (Figure 1b). After a long time $t = \infty$, i.e., $t \gg T_M$, where $T_M = \eta/G$ is the Maxwell time defined as the ratio of η to rigidity G , the system is completely relaxed, and the displacement (Figures 1d and 1e) is the same as that of an elastic plate on top of an inviscid fluid (Figure 1c). However, at an intermediate time $0 < t < \infty$ (e.g., t_1 or t_2 in Figure 1d), displacement for a system with a less viscous mantle (Figure 1d) is closer to the completely relaxed state than that with a more viscous mantle (Figure 1e). This means that stress in the system with a lower viscosity relaxes faster than that with a higher viscosity. It can be shown that in linear Maxwell viscoelastic deformation, timescales with viscosity and hence the Maxwell time. Obviously, the system with a lower viscosity has a faster surface deformation rate (velocity) after the earthquake.

[4] For an imposed earthquake deformation, the incremental stresses in the elastic plates do not relax unless stresses in the viscoelastic neighbor (the upper mantle) do. The relaxation of the viscoelastic upper mantle and its interaction with the elastic plates lead to material

flow. When the flow ceases depends on the mantle viscosity.

2. Tectonic Setting and GPS Observations

2.1. Tectonic Setting and the 1960 Great Earthquake

[5] At the Chile margin, the Nazca plate subducts beneath South America (Figure 2). The age of the subducting plate is greater than 30 Ma at the 37°S latitude and becomes much younger to the south toward the subducting Chile Ridge around latitude 47°S. Large thrust earthquakes have ruptured almost every part of this plate boundary over the past 100 years [Kelleher, 1972].

[6] Plate kinematics provides a first-order control on subduction earthquake processes, but there is some uncertainty regarding the relative plate convergence rate at this margin. The NUVEL-1a model of global plate motion [DeMets *et al.*, 1994] predicts the long-term Nazca-South America convergence rate to be 80 mm/yr in a direction of N81°E at the 32°S latitude. However, for the same latitude, Angermann *et al.* [1999] suggested a contemporary rate of 66 mm/yr (directed N80°E) based on data from two GPS campaigns in 1994 and 1996 involving four sites on the Nazca plate and five sites defining a stable core of the South

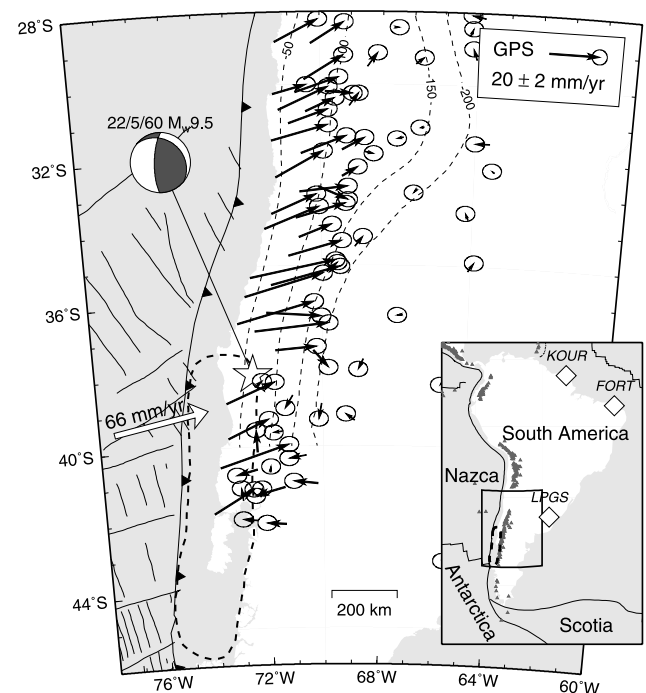


Figure 2. Tectonic setting of the Chile margin and GPS velocities [Klotz *et al.*, 2001; Khazaradze *et al.*, 2002]. Thick dashed line approximates the rupture zone of the M_w 9.5 1960 earthquake [Plafker, 1972]. Epicenter of the 1960 earthquake [Cifuentes, 1989] is marked with a star. The thin dashed contour lines indicate depths to slab surface in km. Offshore NW and NE trending lines represent magnetic lineation and transform faults, respectively. Inset shows the large-scale tectonic environment, with the three GPS stations used to define a South America reference for the GPS velocities indicated by open diamonds and volcanoes indicated by gray triangles.

America plate. *Angermann et al.* [1999] argued that the rate based on GPS observations indicates that the convergence has slowed down over recent geological time. For modeling deformation associated with recent earthquakes, the contemporary convergence rate is preferred [*Klotz et al.*, 2001], but uncertainties in the GPS measurements must also be taken into consideration.

[7] The largest instrumentally recorded earthquake on Earth occurred at this margin on 22 May 1960, with a moment magnitude $M_w = 9.5$ [*Kanamori*, 1977]. *Cifuentes* [1989] estimated the rupture length of the main shock, consisting of two subevents, to be 920 ± 100 km. On the basis of amplitude measurements of low-frequency (1.0–5.0 mHz) normal mode data, a line source propagating at a constant rupture velocity was used to obtain a source model consisting of three subevents [*Cifuentes and Silver*, 1989].

[8] The 1960 rupture propagated about 900 km southward from the hypocenter and a short distance northward (Figure 2). Coseismic land-level changes range from 5.7 m of uplift to 2.7 m of subsidence [*Plafker and Savage*, 1970]. *Plafker* [1972] deduced a rupture zone 120 km wide and 1000 km long dipping 20° with 20 m of slip from coseismic deformation data. *Barrientos and Ward* [1990] developed an inversion model to infer the coseismic fault slip distribution from surface deformation data. In their spatially variable fault slip model, the slip varies from 0 to 40 m. If the slip was assumed to be uniform along a rectangular fault 850 km long, 130 km wide, and dipping at 20° , they obtained an average slip of 17 m.

[9] There are various reports of aseismic fault slip in association with the 1960 event. *Linde and Silver* [1989] suggested that the uplift data of *Plafker and Savage* [1970] not only reflect coseismic deformation of the 1960 earthquake, but also aseismic slip downdip of the rupture zone in a 60–85 km depth range, possibly preceding the main rupture. *Nelson and Manley* [1992] reported that a small island, Isla Mocha, had an uplift of 1.4 m and 1.76 m during 1960–1965 and 1965–1989, respectively. Isla Mocha is located around latitude 38.2°S about 40 km offshore and is directly above the 1960 rupture zone (Figure 2). If the rupture zone is locked after the earthquake, the island should only experience subsidence. The uplift has been attributed to aseismic slip of a thrust fault in the upper plate or a segment of the subduction fault [*Nelson and Manley*, 1992]. On the basis of tide gauge records up to 1989, *Barrientos et al.* [1992] reported at least 0.75 m postseismic uplift around latitude 41.2°S and interpreted it as due to postearthquake aseismic slip downdip of the 1960 rupture zone in the 50–90 km depth range.

2.2. GPS Observations Along the Chilean Margin

[10] The Chile subduction zone has been extensively surveyed using GPS [*Norabuena et al.*, 1998; *Bevis et al.*, 1999; *Klotz et al.*, 1999, 2001]. Starting in 1993, the GeoForschungsZentrum (GFZ) Potsdam, Germany, within the framework of South American Geodynamic Activities (SAGA) project and in cooperation with numerous local host organizations, established a large-scale GPS campaign network in Chile and western Argentina. Velocities have been derived at more than 200 sites in an area of about 2500 km long along the margin and 800 km wide [*Klotz et al.*, 2001; *Khazaradze and Klotz*, 2003]. Results from the

southern half of this network based on two GPS surveys in 1994 and 1996 separated by 2.6 years are shown in Figure 2. Data from another survey in 2000 are yet to be processed. During each GPS campaign, each site was occupied for at least three consecutive days with daily observation periods of more than 20 hours. All the campaign data, together with data from selected International GPS Service (IGS) sites and the GFZ permanent GPS stations in South America, were processed using GFZ software EPOS (Earth Parameter and Orbit System) that uses undifferenced phase and pseudorange observables [*Angermann et al.*, 1997].

[11] Site coordinates and velocities were derived in three steps. (1) All the data were processed simultaneously without constraints using the combined IGS satellite orbits and the Earth orientation parameters to obtain fiducial-free station coordinates. (2) The processed solution was transformed into the International Terrestrial Reference Frame (ITRF97). (3) The ITRF97 solution was then transformed into a regional reference frame. The regional reference frame is fixed to a nominal “stable” South America that is defined using IGS stations KOUR, FORT, and LPGA (Figure 2 inset). No other constraints were imposed. The achieved regional network precision ranges between 2–4 and 5–7 mm for horizontal and vertical components, respectively. Given the poor vertical precision, two observations separated by 2 years are not sufficient to resolve vertical motion with adequate confidence in most of the study area. Hence in this study we only consider the horizontal components of the GPS velocities.

[12] There are three prominent features in the GPS observations in Figure 2. First, all the coastal sites are moving landward, indicating that the thrust interface is currently locked. Second, the landward velocities in the coastal region at the latitudes of the 1960 earthquake are distinctly smaller than those to the north. The third and the most intriguing feature is that from 38°S to 42°S , a group of inland sites about 200–400 km from the trench are moving seaward. *Klotz et al.* [2001] qualitatively attributed this opposite motion to postseismic relaxation effects of the 1960 great earthquake. Our modeling will address all the above first-order features, but the seaward motion of the inland sites is the primary focus.

2.3. Processes Responsible for the Seaward Motion of Inland GPS Sites

[13] The above mentioned seaward motion of inland sites cannot be an artifact for the following reasons. It is unlikely due to an error in the reference frame because all the GPS data in Figure 2 were processed using the same procedure and referenced to the same nominal stable South America plate. It cannot be due to random errors because a contiguous subset of stations shows the same sense of motion. The coherent pattern of seaward motion occurs only landward of the rupture region of the great 1960 earthquake, suggesting a causal link. Seaward motion of inland sites landward of a great earthquake rupture area is not unique to this margin. Similar seaward crustal motion was reported at the Alaska subduction zone about 300–400 km from the trench [*Frey Mueller et al.*, 2000; *Savage et al.*, 1999], and the motion spatially correlates with the rupture region of the great 1964 earthquake of M_w 9.2. Candidate mechanisms responsible for the seaward motion

include deep aseismic fault slip and viscoelastic stress relaxation.

[14] An interplate great earthquake may induce aseismic afterslip of the fault downdip of the rupture segment that may continue for sometime after the event. *Zweck et al.* [2002] explained the present-day seaward motion of inland GPS sites at the Alaska subduction zone by proposing afterslip in a purely elastic Earth model that lasted at least for several decades. *Sato et al.* [2003] showed that some viscoelastic stress relaxation is also required to explain these observations.

[15] It is generally difficult to distinguish between contributions to postseismic deformation from fault afterslip and mantle relaxation [*Pollitz et al.*, 1998; *Wang*, 2004], but it is usually assumed that transient fault slip may be important for a timescale of months to years, and viscoelastic stress relaxation is important for a timescale of decades to centuries. It is clear that the timescale for significant afterslip of a downdip extension of the rupture zone of the 1994 Sanriku-oki earthquake off NE Japan is indeed very short, no more than two years [*Uchida et al.*, 2003] or even within 100 days after the earthquake [*Yagi et al.*, 2003]. The afterslip slows down or stops afterward.

[16] In addition to the timescale consideration, to use the afterslip model to explain the GPS data at the Chile margin would require a very deep slip zone because of the large distance of the seaward moving GPS stations to the 1960 rupture zone. *Hu* [2004] conducted simple tests using a 3-D model of dislocation in a uniform elastic half space [*Okada*, 1985] to assess spatial relations between the seaward motion of inland GPS sites and possible long-term afterslip at the Chile margin. He found that, unlike at the Alaska margin where the slab dips shallowly, the afterslip segment at the Chile margin would have to be over 100 km deep and below the volcanic front in order to explain the seaward motion. It is questionable whether an elastic fault model is applicable at such depth where deformation along the plate interface is expected to be ductile because of the high temperatures. If a shallower afterslip zone was assumed, no reasonable afterslip rate could be found to match simultaneously the GPS patterns in both the landward moving coastal area and the seaward moving inland area. Therefore prolonged afterslip in a purely elastic Earth is unlikely to be a dominant mechanism for the seaward motion of the inland area for this margin. *Barrientos et al.* [1992] assumed afterslip in a 50–90 km depth range downdip of the 1960 Chile earthquake rupture in order to explain postseismic uplift indicated by tide gauge observations within 30 years of the earthquake, but as we will demonstrate subsequently, the uplift may alternatively be explained as due to viscoelastic stress relaxation.

[17] Downdip of the seismogenic zone, a subduction fault may slip aseismically and episodically during the interseismic period [*Dragert et al.*, 2001; *Ozawa et al.*, 2002]. Such slip may cause brief episodes of seaward motion of GPS stations. The physical mechanism of these silent events is not understood and is under intense investigation. The depth range of these slips is about 30 to 50 km. An elastic model of silent slip that explains the seaward motion of GPS sites at the Chile margin will be similar to the afterslip model except for a different time of slip occurrence. Therefore it

has the same requirement for a deep slip zone, which is at odds with all silent slip observations and models.

[18] Viscoelastic stress relaxation, as explained in the Introduction, is our preferred mechanism. We have published some preliminary results of a 3-D viscoelastic finite element model to explain the GPS observations [*Khazaradze et al.*, 2002]. In the present paper, we present a revised model and a much more detailed investigation of the mechanical process. As we will demonstrate subsequently, the same process also explains the second feature of the GPS observations (section 2.2), i.e., the amplitude contrast of coast velocities between the region of the 1960 earthquake and the area to the north. This strengthens our contention that viscoelastic stress relaxation is a fundamental process common to all large earthquakes. Only two subduction earthquakes (1960 Chile, 1964 Alaska) recorded in the past century have moment magnitude above 9 and rupture zones over 900 km long. It is probably not a coincidence that in both cases seaward crustal motion has been observed landward of the rupture region several decades after the events. In a 3-D viscoelastic finite element model of Cascadia great subduction earthquake cycles [*Wang et al.*, 2001], there was a seaward motion of inland sites 50 years after the 1700 great earthquake that was also estimated to be $M_w \sim 9$.

3. Finite Element Model

3.1. Geometry

[19] Finite element models that include the heterogeneity of the real Earth may produce a good fit to crustal deformation observations. However, the purpose of this work is to study the first-order postseismic deformation, and fine details of the heterogeneity are ignored. Simplifications allow us to focus on the essential aspects of the fundamental physical process. Our model consists of an elastic upper plate, an elastic subducting plate including the slab, a viscoelastic oceanic mantle, and a viscoelastic continental mantle, as schematically shown in Figure 1a. The material is assumed to be uniform within each of these tectonic units. The x axis is northward positive in the strike direction (N3.2°E). The y axis is landward positive.

[20] The elastic over-riding plate includes the crust and the lithospheric mantle. The effective elastic thickness of old continental lithosphere is estimated to be 35–40 km [*Burov and Diament*, 1995]. This thickness may not be uniform. The very low heat flow in subduction zone forearcs may make the elastic thickness larger, and high heat flow in the volcanic arc and back arc may make the thickness smaller. We assume a thickness of the elastic continental upper plate of 40 km, but uncertainty in this choice is large. Other values will be tested for sensitivity analysis. The thickness of the elastic oceanic plate (including the subducting slab) is assumed to be 30 km as in the work of *Khazaradze et al.* [2002], consistent with the elastic thickness of an oceanic plate of 20–30 Ma age [*Watts and Zhong*, 2000]. Changing this value by 10 km makes little difference to model results for the region of GPS measurements.

[21] The shape of the subducting slab is based on published slab contours [*Dewey and Lamb*, 1992; *Cahill and Isacks*, 1992]. A generalized shape of the subducting slab is obtained by fitting these data with a parabolic function. The

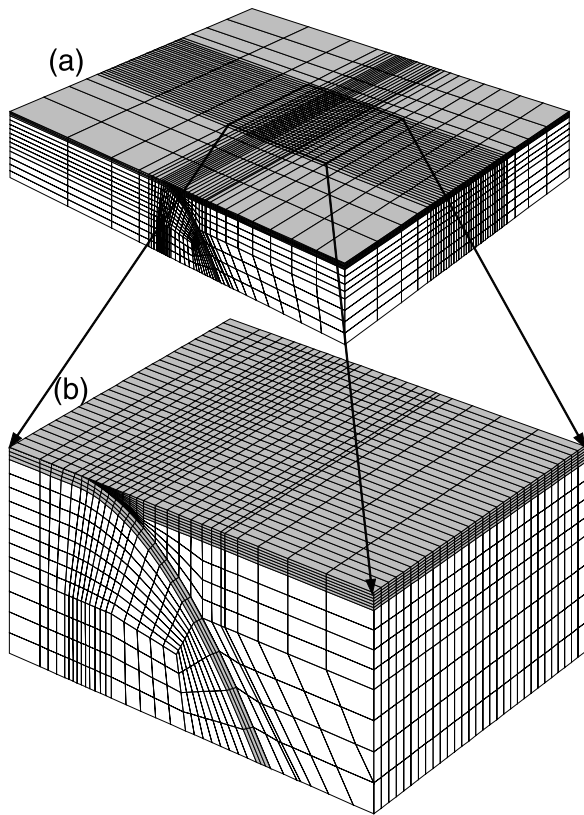


Figure 3. Finite element mesh used in this work: (a) entire mesh and (b) center part. Shaded parts are elastic plates, and the rest is the viscoelastic mantle. For the reference model the mesh is 3000, 1300, and 500 km in the strike, trench-normal, and vertical directions, respectively.

resultant 2-D slab shape is then used for all the trench-normal profiles of the 3-D model. The simplification that all trench-normal cross sections are identical is consistent with the fact that there is little observed variation of the slab geometry south of 35°S. The younger age of the subducting plate may lead to a decrease in slab dip toward the triple junction around 47°S, but there is no observation to constrain it.

[22] We construct a finite element mesh that conforms to the expected geometry of the subduction zone (Figure 3). The bottom of the mesh is set at 500 km depth, in the middle of the mantle transition zone. Except for the free upper surface, displacement perpendicular to each model boundary is fixed to be zero, and displacements parallel to the boundary are not constrained. The mesh extends from 650 km seaward of the trench to 650 km landward of the trench and is 3000 km long in the along-strike dimension. There are a total of 27,170 trilinear eight-node elements, with grid spacing ranging from 0.4 km around the subduction fault to over 200 km at the model boundaries.

3.2. Prescribed Fault Slip

[23] The slip on the fault is kinematically prescribed using the split-node method [Melosh and Raefsky, 1981]. In this work, the earthquake is modeled as an instantaneous uniform slip of 20 m in the plate convergence direction over a rectangular rupture zone 900 km long and 120 km wide

(dark area in Figure 4b). In plan view, the rupture zone is at the center of the model domain. The size of the rupture zone and the amount of slip are similar to those assumed by *Plafker* [1972]. If we allow the rupture to terminate abruptly at its downdip edge, the model-predicted coseismic uplift/subsidence pattern (not shown here) is also very similar to the results that *Plafker* [1972] obtained using a dislocation model with a planar fault. *Plafker* [1972] showed that this pattern compared quite well with observations reported by *Plafker and Savage* [1970], indicating that the downdip termination of the coseismic slip was probably very abrupt. The inversion results of *Barrientos and Ward* [1990] are also consistent with an abrupt termination.

[24] Although prolonged afterslip downdip of the rupture zone is unlikely to have been a prominent process at the Chile margin, we think significant afterslip must have immediately followed the earthquake, as in the case of the Sanriku-oki earthquake of 1995 discussed in section 2.3. “Preslip” downdip of the rupture zone immediately before the event has also been suggested [Linde and Silver, 1989]. Our finite element model simulates deformation in response to prescribed fault slip, not stress-dependent fault slip itself [Dieterich, 1978]. For simplicity and considering that the focus of the study is the decadal postseismic deformation, we include the effects of transient afterslip and any possible preslip in the coseismic step by adding an 80 km wide zone of transition downdip of the rupture zone (gray area in Figure 4b), over which the slip linearly decreases to zero. Changing the width of the transition zone to 40 km has a very small effect on the results [Hu, 2004]. Similar transitions of 50 km width in the strike direction are added to the northern and southern edges of the fault to avoid abrupt termination of the coseismic rupture in these places.

[25] After the earthquake, the rupture zone is assumed to be fully locked, and the coseismic downdip transition zone

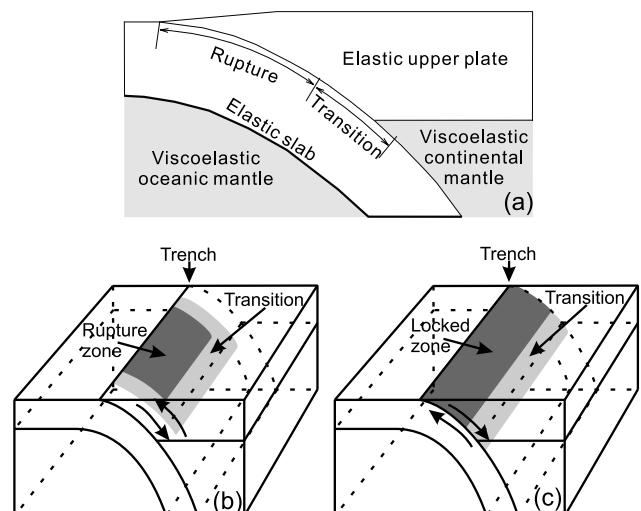


Figure 4. (a) Conceptual representation of the fault model of this work. (b) Coseismic slip model of the 1960 earthquake. (c) Back slip model for fault locking after the earthquake. Slip in Figure 4b or back slip rate in Figure 4c tapers to zero over the transition zone. In the downdip direction, the rupture/locked zone is 120 km wide, and the transition zone is 80 km wide.

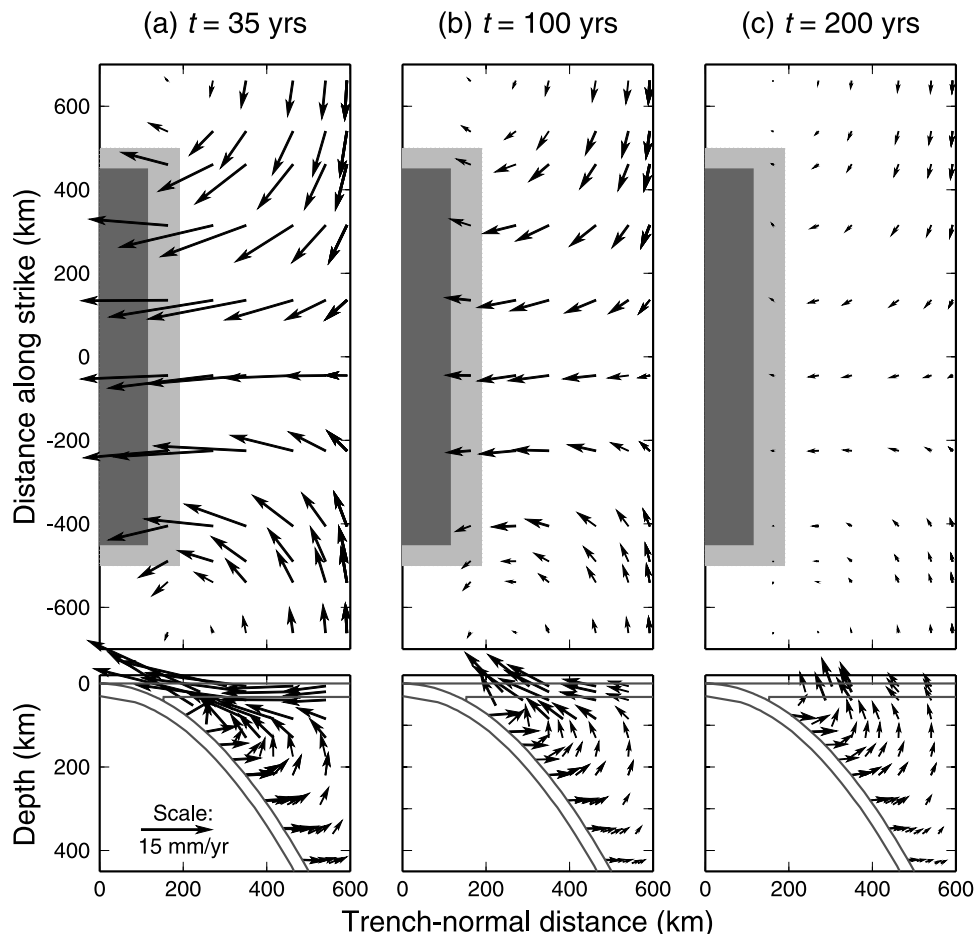


Figure 5. Velocities in response to the earthquake alone without subsequent fault locking. Upper panels show the surface velocities in plan view, with surface projections of the rupture and transition zones indicated by dark and light shading, respectively. Lower panels are cross sections along the line of symmetry of the model, with the elastic plates outlined with solid lines.

becomes the interseismic transition zone. The 1960 earthquake only ruptured a segment of the Chilean margin, but the Chilean subduction fault is believed to be locked along its entire length at present. Therefore the locked and interseismic transition zones are extended from the rupture zone to the northern and southern mesh boundaries as shown by the dark and gray areas in Figure 4c. The locking of the fault is modeled using the method of back slip [Savage, 1983]. A back slip at the plate subduction rate assigned to the locked zone represents a fully locked fault. Over the downdip transition zone, the back slip rate linearly decreases to zero. If the subduction process is assumed to be purely seismic, it will take 300 years to accumulate enough slip deficit for the next 20-m rupture event with a back slip rate of 66 mm/yr, or 250 years with a rate of 80 mm/yr. The convergence rate of 66 mm/yr is used, but a faster rate will also be tested.

3.3. Material Properties

[26] Following Wang *et al.* [2001], the Young's modulus of the elastic plates and mantle are assumed to be 120 GPa and 160 GPa, respectively, and the Poisson's ratio and rock density are assumed to be 0.25 and 3.3 g/cm³, respectively, for the entire system. The gravitational acceleration is

assumed to be 10 m/s². Gravity is not directly modeled as a body force, but its effect of tending to bring a perturbed system back to the hydrostatic state is modeled using a prestress advection approach [Peltier, 1974; Wang *et al.*, 2001].

[27] Assuming a viscosity of 2.5×10^{19} Pa s and a Young's modulus of 160 GPa, the mantle Maxwell relaxation time is ~ 12 years. Justifications for this viscosity value will be discussed later. Although there are earthquakes in 1737 and 1835 in this area [Nishenko, 1985], the last great earthquake of comparable size to the 1960 event occurred in 1575 [Atwater *et al.*, 2003]. The almost 400 years time interval between the two great earthquakes is much larger than the Maxwell relaxation time. We assume that the stress induced by the 1575 earthquake was largely relaxed in 1960 and that the effects of the 1737 and 1835 events are small. Therefore previous earthquakes are not included in the model.

[28] The model with parameters described above is called the reference model. Various changes will be made to the reference model for sensitivity tests. The effects of the earthquake and of the subsequent locking of the fault are modeled separately. The combined effect of the earthquake and fault locking is obtained using a linear combination of the results of the two models (Figure 4). We

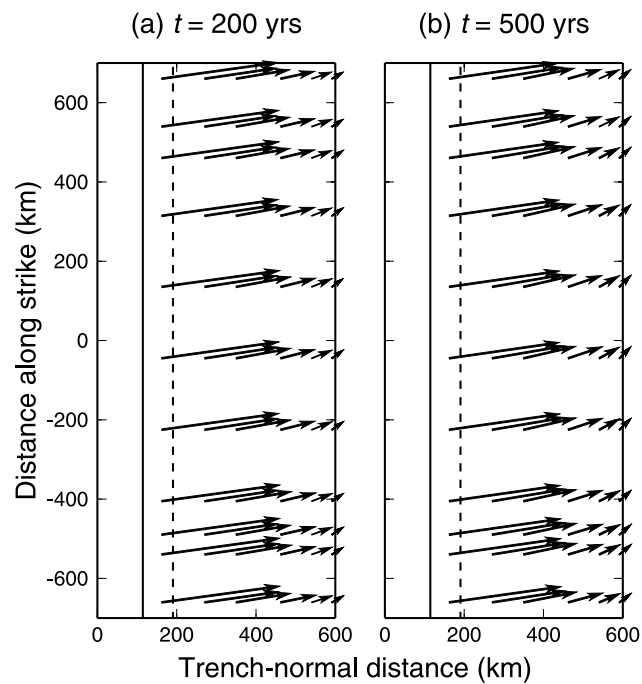


Figure 6. Surface velocities in response to fault locking alone. Back slip begins at time zero. Surface velocities change very little after 200 years. Fault locking effect is represented by the 500-year results. Surface projections of the locked and transition zones are outlined with solid and dashed lines, respectively.

think that the only way to explain the mechanism clearly is to discuss the earthquake and fault-locking effects separately as follows.

4. Model Results

4.1. Deformation Due to the Earthquake Alone

[29] The system's response to the earthquake is modeled by prescribing an instantaneous coseismic slip on the fault without subsequent fault locking. That is, the relative displacements of the nodes on the full-rupture zone of the fault are fixed at 20 m with no subsequent back slip.

[30] The earthquake instantaneously stretches the forearc and induces a shear stress in the mantle. Note that the "stretch" is incremental to a background stress field and does not represent absolute stress. The incremental stretching force tends to pull the rest of the upper plate to move seaward, but the induced shear stress provides a resistance to this motion. As discussed in the introduction, if the upper mantle were purely elastic (viscosity $\eta = \infty$), the resistive stress would never relax, and deformation in response to the earthquake would always be confined to a small area around the rupture. However, also as discussed in the Introduction, if the upper mantle were a pure fluid with no shear strength (viscosity $\eta = 0$), no stress would be induced in the upper mantle, and the crustal deformation would instantaneously extend to a large distance. The mantle viscosity of 2.5×10^{19} Pa s represents intermediate behavior, as in Figure 1d.

[31] The instantaneous stretch of the forearc and the subsequent stress relaxation cause seaward velocities in

areas landward of the trench (Figure 5). In this paper, all model velocities are relative to the fixed model boundaries. The seaward velocities decrease with time as the stretching stress in the elastic plate decreases. The surface velocities landward of the rupture zone along the line of symmetry are slightly oblique because of the oblique plate convergence at Chile, but the strike-parallel component quickly diminishes (Figures 5b and 5c). Displacement (not shown) is first limited to near the rupture but gradually involves a broader landward area [Hu, 2004].

4.2. Deformation Due to Fault Locking Alone

[32] The response to ongoing subduction with the plate interface fully locked is modeled by imposing a back slip rate of 66 mm/yr without a preceding earthquake. As explained in section 3.2, the back slip is assigned to locked and transition zones that extend to the northern and southern boundaries of the model, instead of just the 1960 rupture region. The response to fault locking alone is simply the deformation of a completely relaxed system subject to the constant back slip rate [Savage, 1983; Thatcher and Rundle, 1984; Matsu'ura and Sato, 1989]. In a numerical model, the fault begins to slip backward at time $t = 0$, and the surface velocity increases with time. The system is relaxed in about $20T_M$. For a mantle viscosity of 2.5×10^{19} PA s, the surface velocity field is stabilized after about 200 years (Figure 6). We use the results for $t = 500$ years shown in Figure 6b. For an elastic plate on top of a completely relaxed mantle, the surface velocities should linearly decrease landward. Deviation from the strictly linear trend is caused by the complex geometry of the subduction zone. In addition, if the model boundary 650 km east of the trench is placed farther away, the landward velocity decrease will be more gradual, but the effect is small.

4.3. Deformation Due to the Earthquake As Well As Fault Locking

[33] The response to an earthquake followed by fault locking is obtained by combining the earthquake effect with the fault locking effect. Result for each time step of the earthquake-alone model shown in Figure 5 is combined with the same 500-year result of the back slip model shown in Figure 6b. The combined results are shown in Figure 7. The coseismic slip induces a seaward velocity that decreases with time, but fault locking causes a small landward velocity that does not change with time. The combined effect depends on the balance of these contributions. Earlier in the earthquake cycle (e.g., 35 years and 100 years), the effect of the earthquake dominates in areas landward of the rupture zone. North and south of the rupture zone, the effects of fault locking always dominate, maintaining large landward velocities. Later in the cycle, earthquake-induced shear stress in the upper mantle is mostly relaxed, and hence the effect of fault locking becomes dominant. This leads to an increase in landward velocities (Figures 7b and 7c) in the area landward of the rupture zone.

4.4. Comparison With GPS Observations

[34] In order to compare the model results with GPS campaign data, the GPS data on the surface of the spherical earth are mapped into the Cartesian reference frame of the model using Lambert Conformal Conical projection, with

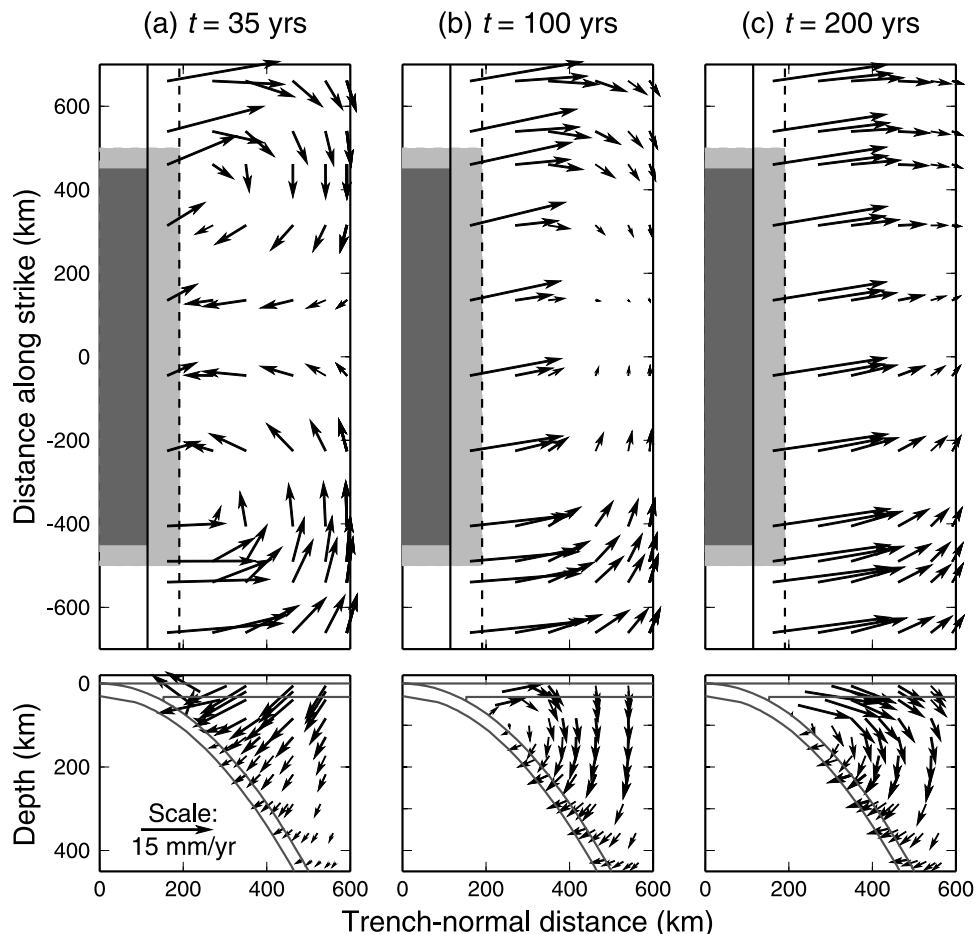


Figure 7. Velocities in response to the earthquake followed by fault locking (i.e., combination of results shown in Figures 5 and the velocities in Figure 6b). Upper panels show the surface velocities in plan view, with surface projections of the rupture and coseismic transition zones indicated by dark and light shading, respectively, and those of locked and interseismic transition zones outlined with solid and dashed lines, respectively. Lower panels are cross sections along the trench-normal line of symmetry of the rupture zone, with the elastic plates outlined by solid lines.

the origin of the Cartesian system placed at $75.6^{\circ}\text{W}/41.5^{\circ}\text{S}$. Figure 8a shows the plan view surface velocities predicted by the reference model (continental mantle viscosity of 2.5×10^{19} Pa s) and GPS observations 35 years after the event. Our simplified model geometry assumes a straight trench, but the strike direction of the trench is slightly more easterly north of the 1960 rupture zone. A straight fault over-predicts the distance between GPS sites and the position of the locked zone in that area. To compensate for this effect, a small distance correction has been made in Figure 8a for the model velocities north of 38°S , such that the same E-W distance from the trench as the actual GPS site is used to calculate the model velocity.

[35] Given the simplicity of the model and uncertainties in the GPS data, the model explains the first-order pattern of the observed velocities reasonably well. Not only the coexistence of the landward motion of the coastal area and the seaward motion of the inland area is reproduced in the model, but also the contrast in coastal velocities between the 1960 rupture region and the area to the north. The coastal velocities at the 1960 rupture latitudes are smaller because, 35 years after the earthquake, they are still

quite strongly affected by postseismic deformation due to stress relaxation, as shown in Figure 7a. One could readily achieve an even better fit to the GPS velocities in the northern area by using a slightly wider locked zone there [Hu, 2004], but we refrain from pursuing a further refined fit because it is the velocity contrast between the two areas that is important to the main purpose of this paper. It is remarkable that, without any ad hoc adjustment of geometrical and fault slip parameters, subtle details such as the spatial change in the direction of inland GPS velocities between 37°S and 39°S are also reproduced by the model (Figure 8a). The average difference between model velocities and GPS observations south of latitude 38°S is 4 mm/yr, comparable to the 2σ errors of the GPS velocities [Klotz *et al.*, 2001]. Since the main objective of the study is to propose and test a process, it is less meaningful to pursue a more precise data fit. Increasing or decreasing the mantle viscosity leads to surface velocities less consistent with GPS observations, an effect that will be discussed in the following section.

[36] This model further predicts that, 70 years after the earthquake, the seaward motion of the inland area will

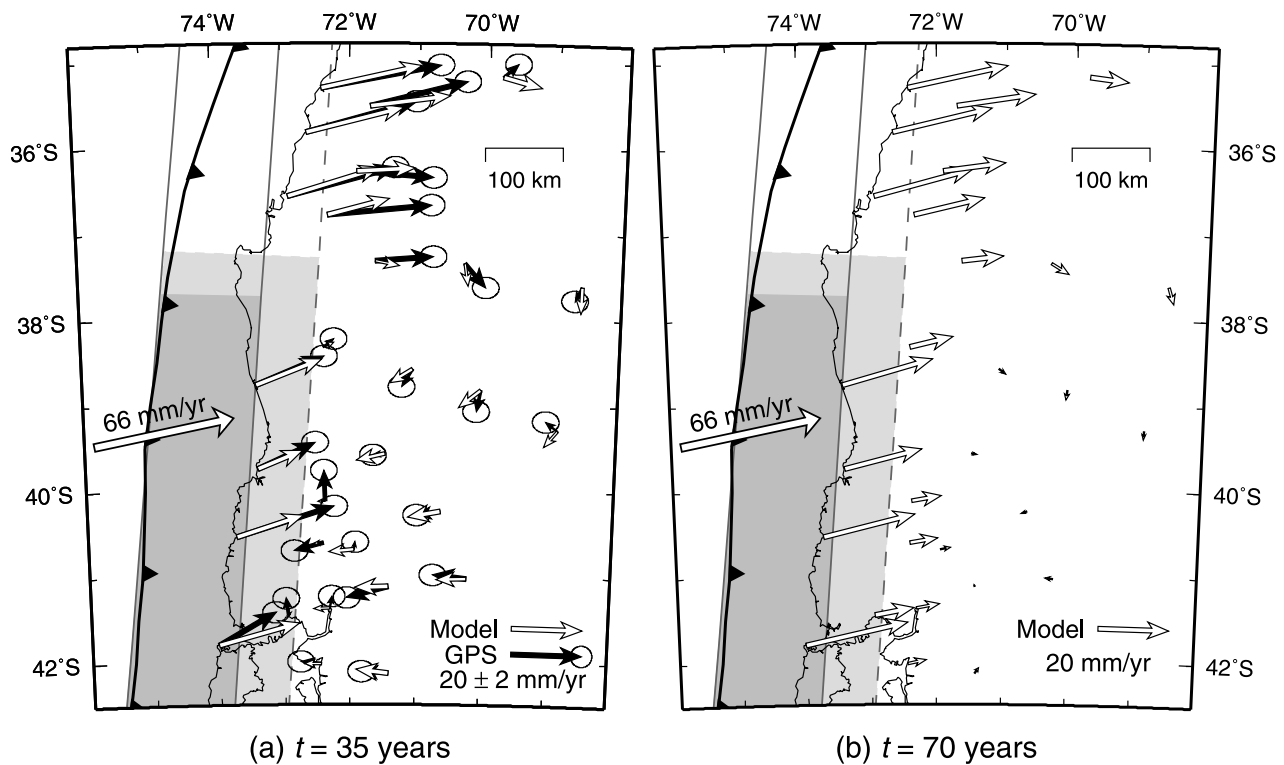


Figure 8. (a) Comparison of velocities calculated using the reference model 35 years after the earthquake and GPS observations. Dark and light shading represent the rupture and coseismic transition zones, respectively. Solid and dashed straight lines outline the locked and interseismic transition zones, respectively. (b) Velocities calculated at the GPS sites 70 years after the earthquake using the same model. By this time, seaward motion of inland GPS sites has nearly stopped, and landward motion of the coastal sites in the earthquake area is much faster.

essentially disappear (Figure 8b). At this time, coastal velocities for the 1960 rupture region are much larger than at 35 years, and the contrast with the northern area is no longer as distinct.

5. Sensitivity Tests and Discussions

5.1. Viscosity of the Continental Mantle

[37] Using a schematic illustration, we showed in the Introduction that the system's response to a displacement perturbation (e.g., known fault slip) is directly portrayed by the time evolution of the displacement field. If there is no subsequent loading such as back slip, the smaller the upper mantle viscosity the more quickly the displacement reaches a new steady state. If we only consider displacements, time will scale with the viscosity and hence the Maxwell time. The scaling is true also for stress and strain. However, for time derivatives of these quantities such as velocities, the time scaling is not as simple. For example, Figures 1d and 1e indicate that the system with a smaller viscosity has a faster deformation rate (velocity) after the earthquake. Therefore it may take a longer, not shorter, time for the system with a lower viscosity to decrease to a given velocity value. Because we examine velocities instead of displacements, this difference should be kept in mind.

[38] Model results for continental mantle viscosities 1×10^{19} Pa s, 2.5×10^{19} Pa s, and 4×10^{19} Pa s are shown in

Figure 9 at 35 years after the earthquake. Response to fault locking alone is not affected by the viscosity value since the mantle is completely relaxed. Seaward velocities in response to the earthquake alone are larger for a smaller viscosity. A side issue worth pointing out is that the landward velocities near the trench for the total response change with time, being larger than the assigned back slip rate at the early stage but less at the later stage. In other words, the average position of the trench slightly shifts landward with a rate that decreases with time. This is a consequence of the viscoelastic deformation of the system and is not observed in purely elastic models.

[39] Although stress relaxation is faster for a viscosity of 1×10^{19} Pa s, it takes longer for the velocities in the inland area to decrease to values comparable to the GPS observations. Velocities 40 years after the event are found to better fit the GPS observations (not shown). However, a viscosity of 4×10^{19} Pa s better fits the GPS observations at an earlier time, 16 years after the event (not shown). These tests show that the viscosity value of 2.5×10^{19} Pa s used for the reference model is fairly tightly constrained. A small change has a relatively large effect on model velocities and their fit with the GPS data. This viscosity value is consistent with values inferred from previously published studies of crustal deformation at active continental margins (see review by Wang [2004]). However, the preferred value is for the specific model parameters. Changing parameter values will

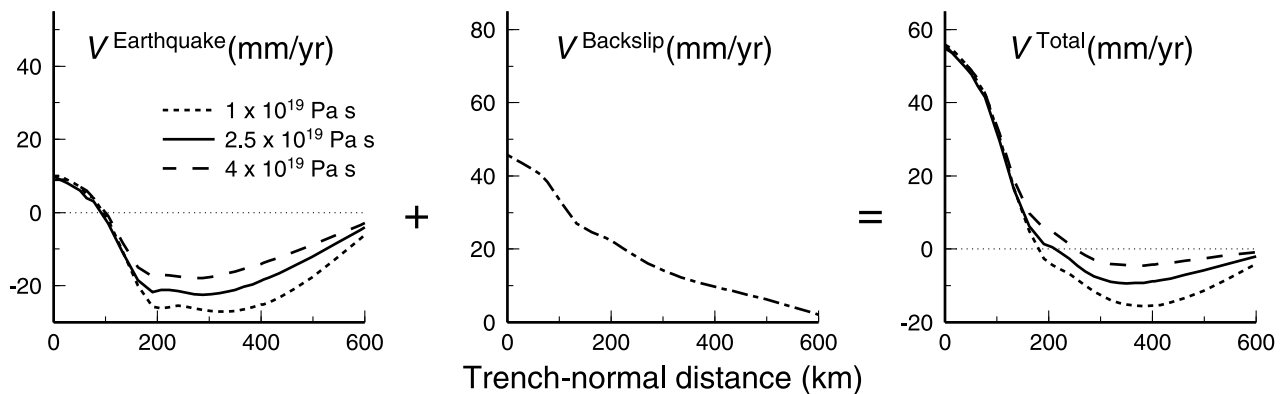


Figure 9. Surface velocities 35 years after the earthquake along the trench-normal line of symmetry of the models for different continental mantle viscosities. Positive velocities indicate landward motion. The viscosity of 2.5×10^{19} Pa s is used for the reference model of Figure 8. $V^{\text{earthquake}}$ is the velocity caused by the earthquake alone. $V^{\text{back slip}}$, velocity due to fault locking alone, is the same for different viscosities because it is the response of the relaxed system.

influence the choice of the viscosity value, but the influence is small, as discussed in the following sections.

5.2. Viscosity of the Oceanic Mantle and Postseismic Uplift

[40] Obviously, stress relaxation that affects surface velocities in the inland area has little to do with the viscosity of the oceanic mantle, although it strongly depends on the viscosity of the continental mantle. We have verified this by changing the oceanic mantle viscosity in the reference model from 1×10^{20} Pa s to the same value of 2.5×10^{19} Pa s as for the continental mantle. The model-predicted surface velocities are almost unaffected (results not shown).

[41] The reason we prefer a higher value for the oceanic mantle is for a postseismic uplift behavior, independent of the horizontal GPS velocities. Postseismic leveling surveys after the 1944/1946 great Nankai, southwest Japan, earthquakes [Thatcher, 1984] and tide gauge records after the 1964 great Alaska earthquake [Cohen and Freymueller, 2001] both indicate that the area of coseismic subsidence quickly became an area of fast uplift after the earthquake. The 0.75 m postseismic uplift up to 1989 that Barrientos *et al.* [1992] inferred from tide gauge records indicates that the Chile margin may have the same behavior. If we use a viscosity of 2.5×10^{19} Pa s for the oceanic mantle, the coseismic subsidence area such as at 200 km from the trench, where Barrientos *et al.*'s [1992] uplift observation approximately apply, does not show significant postseismic uplift (Figure 10). A higher viscosity leads to a quick “rebound”, and over 0.5 m uplift occurs within the first 30 years following the earthquake. The predicted large uplift and decreasing uplift rate with time are in qualitative agreement with Barrientos *et al.*'s [1992] observations. Attempting a more exact fit to the single data point may not be very meaningful, considering potentially large errors in inferring crustal uplift from tide gauge records and possible along-strike variations in uplift rate. Viscoelastic stress relaxation may be a better explanation for the postseismic uplift than the model of prolonged afterslip that requires the slipping segment to extend as deep as 90 km. It is reasonable to assume a continental mantle that is less viscous than the oceanic mantle, because the continental

mantle wedge is expected to be affected by the addition of volatiles from the dehydrating slab.

5.3. Thickness of the Continental Plate

[42] In this test, we change the thickness of the continental plate by 10 km in order to evaluate the effects of the large uncertainty in the choice of the plate thickness of 40 km for the reference model. In Figure 11, we only show the effect of decreasing the thickness by 10 km. Increasing the thickness by 10 km has the opposite effect. The smaller thickness results in greater seaward velocities in response to the earthquake alone (left panel of Figure 11) because of the faster stress relaxation. However, it also results in greater landward velocities in response to fault locking alone (middle panel of Figure 11) because, with a thinner continental plate, the landward shift of the position of the trench as mentioned in section 5.1 is slightly faster. The two opposite effects of assuming a thinner continental plate almost cancel out (right panel of Figure 11). Therefore the uncertainties in the plate thickness do not have a significant impact on model results.

5.4. Faster Plate Convergence or Incomplete Fault Locking

[43] The same parameters as the reference model except for a different interseismic back slip rate are used in this test. The purpose of testing a different rate is two-fold. (1) The value of 66 mm/yr inferred from GPS observations (see section 2.1) has uncertainties. To evaluate the effects of the uncertainties, we compare the results with those obtained by using the NUVEL-1a rate of 80 mm/yr. (2) The calculation of the total slip budget of a subduction fault using the formula of “earthquake slip” = “subduction rate” \times “interseismic interval” is based on an unfounded hypothesis of purely seismic subduction (see Pacheco *et al.* [1993] for a review of seismic versus aseismic subduction). There is not sufficient evidence to determine whether subduction is purely seismic for the Chile margin. The simplest way of accounting for some aseismic component is to assume a constant aseismic slow slip for the interseismic period (i.e., incomplete locking), which translates into a slower interseismic back slip rate [Zheng *et al.*, 1996]. For

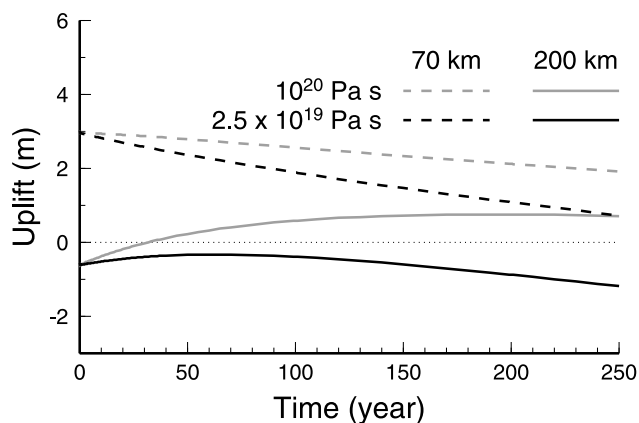


Figure 10. Effect of the oceanic mantle viscosity. Shown is the history of vertical displacement at locations 70 and 200 km from the trench along the trench-normal line of symmetry. The value of 1×10^{20} Pa s is used for the reference model of Figure 8.

example, for a convergence rate of 66 mm/yr, a back slip rate of 52 mm/yr represents an interseismic aseismic slip rate of 14 mm/yr.

[44] Velocities predicted with a back slip rate of 80 mm/yr are shown in Figure 12 along the line of symmetry of the model. The faster back slip rate only affects velocities in response to fault locking; velocities in response to the earthquake alone are the same as in the reference model. The faster back slip rate makes the seaward motion of inland areas slower. To have large enough velocities to fit the GPS data at 35 years after the earthquake, a lower viscosity value of 1.5×10^{19} Pa s is required (comparison with GPS data is not shown). The lower viscosity causes a faster stress relaxation and enhances seaward velocities at these sites.

[45] However, a slower back slip rate, representing incomplete fault locking, will cause larger seaward velocities at the inland sites. Slower stress relaxation, i.e., a higher continental mantle viscosity, will then be needed to compensate for this effect in order to fit the GPS observations. For a convergence rate of 52 mm/yr, a viscosity of $3.5 \times$

10^{19} Pa s gives good fit to the GPS data (results not displayed).

5.5. Rupture Length Along Strike

[46] If a subduction earthquake ruptures a long segment of the plate boundary such as in the cases of the 1960 Chile and 1964 Alaska earthquakes, the coseismic slip causes continuing deformation in a broad area landward of the trench decades after the event. However, if an earthquake ruptures a segment with a short along-strike length, the coseismic slip affects a smaller area near the rupture zone. The earthquake effect will then dissipate more quickly, and the effect of fault locking will more quickly become dominant. We use models with along-strike rupture lengths of 500 km and 200 km to explore this effect (Figures 13a and 13b). For a 200-km rupture, even with an unrealistically large coseismic slip of 20 m, any seaward motion of the inland area at 35 years is much less than those in the reference model that has a 900 km long rupture. The small velocities would be difficult to detect with GPS. A 500-km rupture still has a significant effect. In real subduction earthquakes, coseismic slip tends to be smaller for shorter along-strike ruptures, causing less seaward motion. For example, if a more realistic coseismic slip of 5 m is used for the 200 km rupture model, the earthquake effect completely disappears 35 years after the earthquake (Figure 13c).

[47] Most of the recent subduction earthquakes, such as the 1944 and 1946 Nankai earthquakes, have ruptures less than a couple of hundred kilometers and only a few meters of average coseismic slip, and this explains why seaward motion of inland GPS stations several decades after an earthquake is not more widely observed.

6. Conclusions

[48] The seaward motion of an inland area revealed by campaign GPS data is interpreted to be a delayed response to the great 1960 Chile earthquake. A great thrust earthquake gives rise to an incremental stretching force that drives the upper plate forearc to move seaward, but the shear stress induced in the upper mantle resists this motion and hence limits coseismic displacement to the vicinity of

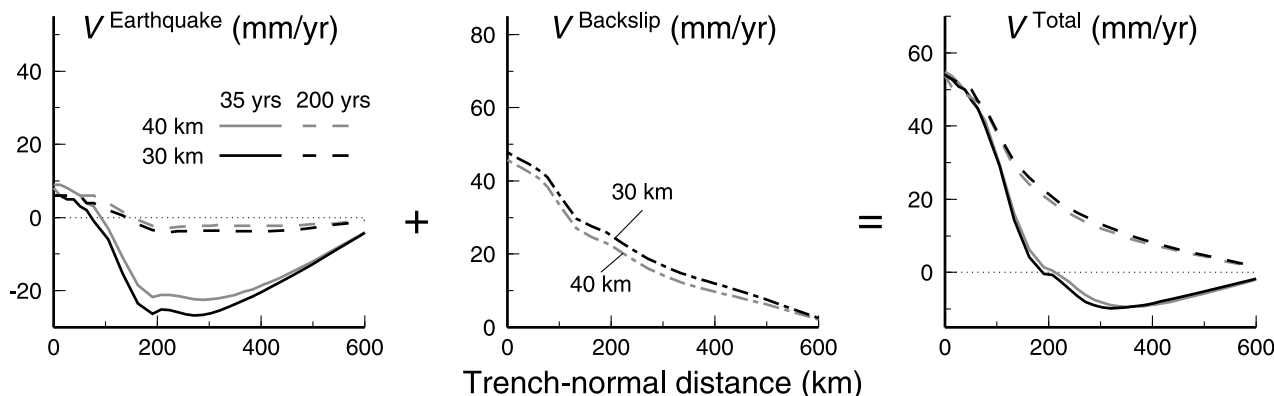


Figure 11. Surface velocities along the trench-normal line of symmetry of the model for different thicknesses of the overriding plate. The thickness of the 40 km is used in the reference model of Figure 8. $V_{\text{earthquake}}$ is the velocity caused by the earthquake alone, and $V_{\text{back slip}}$ is that due to fault locking alone (response of the relaxed system).

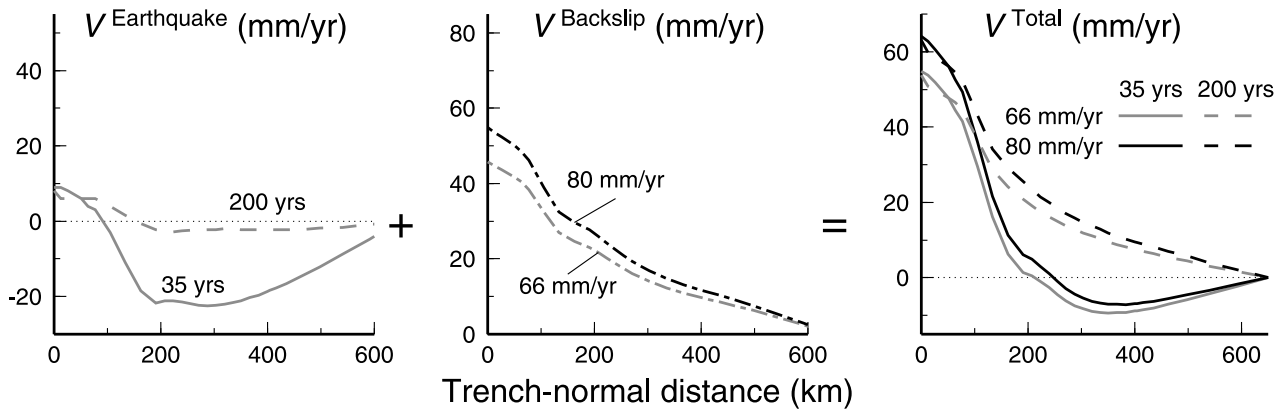


Figure 12. Surface velocities along the trench-normal line of symmetry of the model for different back slip rates. The rate of 66 mm/yr is used in the reference model of Figure 8. $V^{\text{earthquake}}$, velocity caused by the earthquake alone, is independent of the back slip rate. $V^{\text{back slip}}$ is velocity due to fault locking alone (response of the relaxed system).

the rupture area. Subsequent viscoelastic stress relaxation allows the seaward displacement to extend to much larger distances from the rupture zone.

[49] We have developed a 3-D linear Maxwell viscoelastic model to study the postseismic deformation following the 1960 Chile earthquake. The model consists of elastic converging plates and viscoelastic mantle. The earthquake is modeled using a forward slip over the rupture zone. The slip is allowed to decrease to zero over a downdip transition zone to account for the effects of afterslip or preslip downdip of the rupture zone. Because of this approximation, the model results cannot be directly compared with observations made near the coseismic rupture shortly after the earthquake. Fault locking is modeled by assigning a back

slip rate to the locked zone, with back slip at the plate convergence rate representing full locking.

[50] With a continental mantle viscosity of 2.5×10^{19} Pa s, model predicted surface velocities reproduce the first-order pattern of the GPS observations at the Chile margin 35 years after the 1960 earthquake, including landward motion of all coastal sites, smaller landward coastal velocities in the 1960 rupture region as compared to those to the north, and the seaward motion of inland GPS sites. The model shows that at a given time after the earthquake, two competing processes control the direction and magnitude of crustal velocities of the inland area. Relaxation of the earthquake-induced stresses causes seaward velocities that decrease with time. On-going plate convergence with the subduction

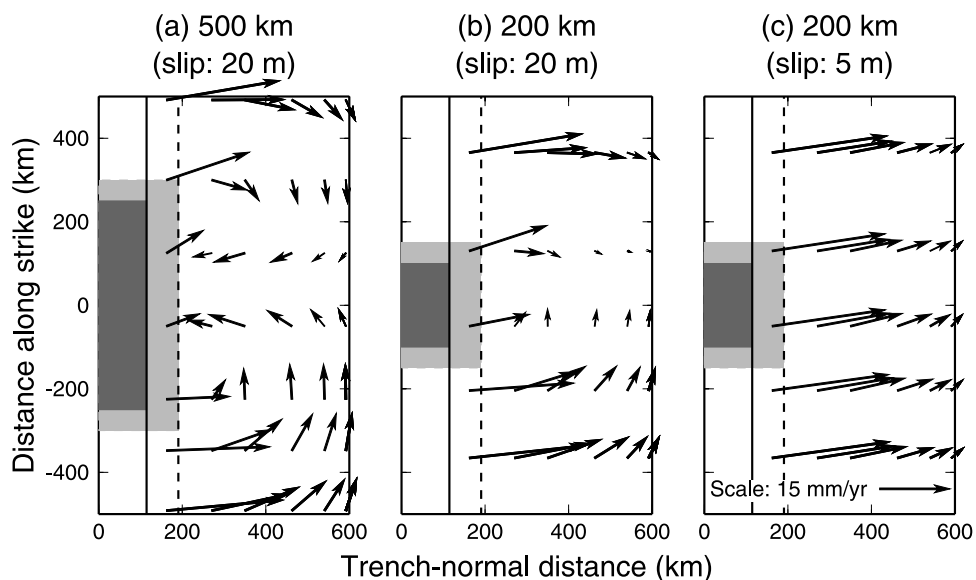


Figure 13. Plan-view surface velocities calculated at 35 years after the earthquake using models with different along-strike rupture lengths and coseismic fault slips as labeled at the top. All other parameters are the same as in the reference model of Figure 8. Dark and light shading represent the rupture and coseismic transition zones, respectively. Solid and dashed lines outline the locked and interseismic transition zones, respectively.

fault locked leads to landward velocities. Not too long after the earthquake, such as 35 years, velocities in the inland area are dominated by the earthquake effect and are in the seaward direction. At later stages, the effect of fault locking becomes predominant, the velocities decrease and eventually change to the landward direction. The model predicts that the seaward motion would disappear into the noise of the surface deformation data 70 years after the earthquake. The model also indicates that if the along-strike rupture length of the earthquake is smaller, such as 200 km, especially if the coseismic fault slip is correspondingly less, such as 5 m, the seaward motion becomes insignificant very quickly after the earthquake. The behavior of the inland area depends on the viscosity of the continental mantle and not on the oceanic mantle, for obvious reasons. However, with a higher oceanic mantle viscosity, the model can also explain postseismic uplift determined from tide gauge records.

[51] Although there is trade-off with other model parameters, the value of 2.5×10^{19} Pa s for the continental mantle viscosity is fairly robust. Increasing or decreasing the value by 1.5×10^{19} Pa s gives much poorer fit to the GPS observations. The model results are not sensitive to the thicknesses of the converging plates. If we increase the back slip rate from 66 mm/yr to the NUVEL-1a convergence rate of 80 mm/yr, a viscosity of 1.5×10^{19} Pa s will fit the GPS data. A lower back slip rate, representing incomplete locking, has the opposite effect. A viscosity value of the order of 10^{19} Pa s is consistent with findings in other subduction margins [Wang, 2004] and the results of postglacial rebound analyses for southern South America [Ivins and James, 1999], but it is in contrast with values of 10^{20} – 10^{21} Pa s assumed in global postglacial rebound models that are more relevant to regions of continental interiors.

[52] **Acknowledgments.** Comments by B. Atwater, W. Thatcher, and D. Schmidt significantly improved the manuscript. YH was partially supported by NSERC grant 227412-01 to KW. Geological Survey of Canada contribution 2004069.

References

- Angermann, D., G. Baustert, R. Galas, and S. Y. Zhu (1997), EPOS.PV3 (Earth Parameter & Orbit System): Software user manual for GPS data processing, *Tech. Rep. STR97/14*, GeoForschungsZentrum, Potsdam, Germany.
- Angermann, D., J. Klotz, and C. Reigber (1999), Space-geodetic estimation of the Nazca-South America Euler vector, *Earth Planet. Sci. Lett.*, *171*, 329–334.
- Atwater, B. F., M. Cisternas, I. Salgado, G. Machuca, M. Lagos, A. Eipert, and M. Shishikura (2003), Incubation of Chile's 1960 earthquake, *Eos Trans. AGU*, *84*(46), Fall Meet. Suppl., Abstract G22E-01.
- Barrientos, S. E., and S. N. Ward (1990), The 1960 Chile earthquake; inversion for slip distribution from surface deformation, *Geophys. J. Int.*, *103*, 589–598.
- Barrientos, S. E., G. Plafker, and E. Lorca (1992), Postseismic coastal uplift in southern Chile, *Geophys. Res. Lett.*, *19*, 701–704.
- Bevis, M., E. C. Kendrick, R. Smalley Jr., T. Herring, J. Godoy, and F. Galban (1999), Crustal motion north and south of the Arica deflection: Comparing recent geodetic results from the central Andes, *Geochem. Geophys. Geosyst.*, *1* doi:10.1029/1999GC000011.
- Burov, E. B., and M. Diament (1995), The effective elastic thickness (T_e) of continental lithosphere: What does it really mean?, *J. Geophys. Res.*, *100*, 3905–3927.
- Cahill, T., and B. L. Isacks (1992), Seismicity and shape of the subducted Nazca plate, *J. Geophys. Res.*, *97*, 17,503–17,529.
- Cifuentes, I. L. (1989), The 1960 Chilean earthquakes, *J. Geophys. Res.*, *94*, 665–680.
- Cifuentes, I. L., and P. G. Silver (1989), Low-frequency source characteristics of the great 1960 Chilean earthquake, *J. Geophys. Res.*, *94*, 643–663.
- Cohen, S. C. (1994), Evaluation of the importance of model features for cyclic deformation due to dip-slip faulting, *Geophys. J. Int.*, *119*, 831–841.
- Cohen, S. C., and J. T. Freymueller (2001), Crustal uplift in the south central Alaska subduction zone: New analysis and interpretation of tide gauge observations, *J. Geophys. Res.*, *106*(B6), 653–668.
- DeMets, C., R. G. Gordon, D. F. Argus, and S. Stein (1994), Effect of recent revisions to the geomagnetic reversal time scale on estimates of current plate motions, *Geophys. Res. Lett.*, *21*(20), 2191–2194.
- Dewey, J. F., and S. H. Lamb (1992), Active tectonics of the Andes, *Tectonophysics*, *205*, 79–95.
- Dieterich, J. H. (1978), Time-dependent friction and the mechanics of stick-slip, *Pure Appl. Geophys.*, *116*, 790–806.
- Dragert, H., K. Wang, and T. S. James (2001), A silent slip event on the deeper Cascadia subduction interface, *Science*, *292*, 1525–1528.
- Freymueller, J. T., S. C. Cohen, and H. J. Fletcher (2000), Spatial variations in present-day deformation, Kenai Peninsula, Alaska, and their implications, *J. Geophys. Res.*, *105*, 8079–8101.
- Hu, Y. (2004), 2-D and 3-D viscoelastic finite element models for subduction earthquake deformation, M.S. thesis, Univ. of Victoria, Victoria, B. C., Canada.
- Ivins, E. R., and T. S. James (1999), Simple models for late Holocene and present-day Patagonian glacier fluctuations and predictions of a geodetically detectable isostatic response, *Geophys. J. Int.*, *138*(3), 601–624.
- Kanamori, H. (1977), The energy release in great earthquakes, *J. Geophys. Res.*, *82*, 2981–2987.
- Kelleher, J. A. (1972), Rupture zones of large South American earthquakes and some predictions, *J. Geophys. Res.*, *77*, 2087–2103.
- Khazaradze, G., and J. Klotz (2003), Short and long-term effects of GPS measured crustal deformation rates along the south-central Andes, *J. Geophys. Res.*, *108*(B6), 2289, doi:10.1029/2002JB001879.
- Khazaradze, G., K. Wang, J. Klotz, Y. Hu, and J. He (2002), Prolonged post-seismic deformation of the 1960 great Chile earthquake and implications for mantle rheology, *Geophys. Res. Lett.*, *29*(22), 2050, doi:10.1029/2002GL015986.
- Klotz, J., et al. (1999), GPS-derived deformation of the central Andes including the 1995 Antofagasta $M_w = 8.0$ earthquake, *Pure Appl. Geophys.*, *154*, 3709–3730.
- Klotz, J., G. Khazaradze, D. Angermann, C. Reigber, R. Perdomo, and O. Cifuentes (2001), Earthquake cycle dominates contemporary crustal deformation in central and southern Andes, *Earth Planet. Sci. Lett.*, *193*, 437–446.
- Linde, A. T., and P. G. Silver (1989), Elevation changes and the great 1960 Chilean earthquake: Support for aseismic slip, *Geophys. Res. Lett.*, *16*, 1305–1308.
- Matsu'ura, M., and T. Sato (1989), A dislocation model for the earthquake cycle at convergent plate boundaries, *Geophys. J. Int.*, *96*, 23–32.
- Melosh, H. J., and A. Raefsky (1981), A simple and efficient method for introducing faults into finite element computations, *Bull. Seismol. Soc. Am.*, *71*, 1391–1400.
- Nelson, A. R., and W. F. Manley (1992), Holocene coseismic and aseismic uplift of Isla Mocha, south-central Chile, *Q. Int.*, *15/16*, 61–76.
- Nishenko, S. P. (1985), Seismic potential for large and great interplate earthquakes along the Chilean and southern Peruvian margins of South America: A quantitative reappraisal, *J. Geophys. Res.*, *90*(B5), 3589–3615.
- Norabuena, E., L. Leffler-Griffin, A. Mao, T. Dixon, S. Stein, S. I. Sacks, L. Ocola, and M. Ellis (1998), Space geodetic observations of Nazca-South America convergence across the central Andes, *Science*, *279*, 358–362.
- Okada, Y. (1985), Surface deformation due to shear and tensile faults in a half-space, *Bull. Seismol. Soc. Am.*, *75*, 1135–1154.
- Ozawa, S., M. Murakami, M. Kaidzu, T. Tada, T. Sagiya, Y. Hatanaka, H. Yarai, and T. Nishimura (2002), Detection and monitoring of ongoing aseismic slip in the Tokai region, central Japan, *Science*, *298*, 1009–1012.
- Pacheco, J. F., L. R. Sykes, and C. H. Scholz (1993), Nature of seismic coupling along simple plate boundaries of the subduction type, *J. Geophys. Res.*, *98*, 14,133–14,159.
- Peltier, W. R. (1974), The impulse response of a Maxwell Earth, *Rev. Geophys.*, *12*, 649–668.
- Plafker, G. (1972), Alaskan earthquake of 1964 and Chilean earthquake of 1960: Implications for arc tectonics, *J. Geophys. Res.*, *77*, 901–925.
- Plafker, G., and J. C. Savage (1970), Mechanism of the Chilean earthquakes of May 21 and 22, 1960, *Geol. Soc. Am. Bull.*, *81*, 1001–1030.
- Pollitz, F. F., R. Burgmann, and P. Segall (1998), Joint estimation of after-slip rate and postseismic relaxation following the 1989 Loma Prieta earthquake, *J. Geophys. Res.*, *103*(B11), 26,975–26,992.
- Sato, H., J. T. Freymueller, and S. C. Cohen (2003), 3-D viscoelastic FEM modeling of postseismic deformation caused by the 1964 Alaska earth-

- quake, southern Alaska, *Eos Trans. AGU*, 84(46), Fall Meet. Suppl., Abstract G21B-0260.
- Savage, J. C. (1983), A dislocation model of strain accumulation and release at a subduction zone, *J. Geophys. Res.*, 88, 4984–4996.
- Savage, J. C., J. L. Svarc, and W. H. Prescott (1999), Deformation across the Alaska-Aleutian subduction zone near Kodiak, *Geophys. Res. Lett.*, 26, 2117–2120.
- Thatcher, W. (1984), The earthquake deformation cycle at the Nankai Trough, southwest Japan, *J. Geophys. Res.*, 89, 3087–3101.
- Thatcher, W., and J. B. Rundle (1984), A viscoelastic coupling model for the cyclic deformation due to periodically repeated earthquakes at subduction zones, *J. Geophys. Res.*, 89, 7631–7640.
- Uchida, N., T. Matsuzawa, and A. Hasegawa (2003), Interplate quasi-static slip off Sanriku, NE Japan, estimated from repeating earthquakes, *Geophys. Res. Lett.*, 30(15), 1801, doi:10.1029/2003GL017452.
- Wang, K. (2004), Elastic and viscoelastic models of crustal deformation in subduction earthquake cycles, in *The Seismogenic Zone Experiment*, edited by T. Dixon, Columbia Univ. Press, in press.
- Wang, K., J. He, H. Dragert, and T. S. James (2001), Three-dimensional viscoelastic interseismic deformation model for the Cascadia subduction zone, *Earth Planets Space*, 53, 295–306.
- Watts, A. B., and S. Zhong (2000), Observations of flexure and the rheology of oceanic lithosphere, *Geophys. J. Int.*, 142, 855–875.
- Yagi, Y., M. Kikuchi, and T. Nishimura (2003), Coseismic slip, postseismic slip, and largest aftershock associated with the 1994 Sanriku-haruka-oki, Japan, earthquake, *Geophys. Res. Lett.*, 30(22), 2177, doi:10.1029/2003GL018189.
- Zheng, G., R. Dmowska, and J. R. Rice (1996), Modeling earthquake cycles in the Shumagin segment, Alaska, with seismic and geodetic constraints, *J. Geophys. Res.*, 101, 8383–8392.
- Zweck, C., J. T. Freymueller, and S. C. Cohen (2002), Three-dimensional elastic dislocation modeling of the postseismic response to the 1964 Alaska earthquake, *J. Geophys. Res.*, 107(B4), 2064, doi:10.1029/2001JB000409.

J. He and K. Wang, Pacific Geoscience Centre, Geological Survey of Canada, 9860 W Saanich Rd., Sidney, BC, Canada V8L 4B2. (kwang@nrcan.gc.ca)

Y. Hu, School of Earth and Ocean Sciences, University of Victoria, Victoria, BC, Canada V8W 3P6.

G. Khazaradze, Department of Geodynamics and Geophysics, University of Barcelona, Barcelona E-08028, Spain.

J. Klotz, GeoForschungsZentrum Potsdam, Kinematics/Neotectonics, Telegrafenberg, Potsdam D-14473, Germany.